CrossMark

ORIGINAL PAPER

Fourier transform infrared spectroscopy to assess molecular-level changes in microorganisms exposed to nanoparticles

Fatemeh Faghihzadeh[1] · Nelson M. Anaya[1] · Laura A. Schifman[1] ·
Vinka Oyanedel-Craver[1]

Abstract Fourier transform infrared (FTIR) is a spectroscopy method that can identify variations in the total composition of microorganisms through the determination of changes in functional groups in biomolecules. FTIR measures the vibration and rotation of molecules influenced by infrared radiation at a specific wavelength. This technique allows the identification of structural changes in the molecular binding between microorganisms and metal atoms, which can provide information about the nature of their interactions. In this review article, we will describe the state of the art in current uses of FTIR for the elucidation of bacteria–nanoparticle interactions. We will describe advantages for the application of FTIR in the field of nanotoxicology, including higher signal-to-noise ratio, high energy throughput, as well as high accuracy and stability which are applicable to solid phase samples but not recommended for assays in the liquid phase. Limitations such as multiple background scans and post-processing analysis are not deniable. Comparison of FTIR with other commonly used tools such as Raman spectroscopy, mass spectrometry, nuclear magnetic resonance spectroscopy, and X-ray photoelectron spectroscopy is also discussed. Finally, we present an application of FTIR for the assessment of bacterial changes in response to the exposure to silver nanoparticles (AgNPs). The results showed that the AgNPs-induced structural changes in the peptide and amino acids region may lead to alterations of conformation and/or composition of Amid B and Amid III. These results showed that bacteria developed resistance toward AgNPs and resulted in changes in the genotype and expression in the phenotype. Here, ATR–FTIR provided the evidence of the AgNPs cytotoxicity-induced intracellular level alterations in bacteria.

✉ Vinka Oyanedel-Craver
    craver@uri.edu

[1]   Department of Civil and Environmental Engineering,
      University of Rhode Island, 1 Lippitt Rd., Bliss Hall 203,
      Kingston, RI 02881, USA

Introduction

Rapid and specific analytical tools to characterize the interactions between bacteria and nanoparticles are essential for the development of safe and effective nanomaterials. These tools can also help to prevent the unintentional negative effects that nanomaterials could have on ecosystems and public health. Broad spectrum molecular analytical tools based on infrared (IR) spectroscopy were introduced in the 1950s [56, 65, 107]. After making several improvements to IR tools, researchers in the 1970s developed Fourier transform IR (FTIR) spectroscopy based on a new computational analysis, which led to Naumann and Helm [47, 89] introducing the FTIR technique for in situ analysis of bacteria. FTIR can identify molecular signatures in bacteria composition due to the absorption of energy in the infrared region. Biochemical bonds are detected based on their molecular rotational degree and type of movement, such as stretching [91, 100], bending [91, 102], scissoring [100, 102], or twisting [91, 100].

FTIR techniques were applied to identify bacteria [56, 65, 107, 125] and classify [47, 76] bacterial strains through the use of spectral libraries for each type of bacteria [77].

These libraries are available as a package through various scientific companies [40]. Furthermore, several studies have shown the capability of FTIR to differentiate between intact and injured cells in stress conditions [3–5, 70, 71, 73].

Recently, FTIR has been used to characterize bacteria exposed to nanoparticles [36, 37, 45, 49, 52, 58, 86, 108, 130, 134]. For instance, FTIR has been used to determine bacterial structural changes after exposure to different types of nanomaterials, such as oxides [49, 52, 58, 86, 134], quantum dots [37], and organic nanoparticles [108].

From a biochemical perspective, it is important to determine interactions at the molecular level as they could provide fundamental information on the effects observed at a systemic level. Due to the technological advances, simplicity of the sample preparation, and high speed of analysis, FTIR spectroscopy could fill the growing demand of fast and reliable toxicity screening in the field of nanotoxicology.

Overview of FTIR fundamentals

The emitted radiation from an IR source passes through an interferometer composed of a beam splitter, a fixed mirror, and a moving mirror (Fig. 1). The interferometer measures the wavelength of emitted light via interference patterns that help to increase accuracy. IR spectra are obtained by applying IR radiation to a sample and measuring the intensity of the passing radiation at a specific wavenumber (Fig. 1). The number of scans can be adjusted based on the quality requirement for the sample analysis; currently, the most common number of scans used is 2^8. IR radiation of certain molecular groups can be detected at a specifics wavenumbers. The x axis of the spectrum represents the wavenumber while the y axis represents absorbance or transmittance [29, 58, 86].

The most common FTIR-based methods for bacteria characterization are transmittance FTIR, attenuated total reflectance (ATR–FTIR), and micro-spectroscopy FTIR.

Transmittance FTIR

FTIR analysis can be carried out in solid, liquid, or gas samples; however, here only solid and liquid phase sample applications will be discussed. Solid samples should be ground with potassium bromide (about 5 % of the weight of the sample) and pressed to form a hard pellet. Then the sample is placed between two infrared–transparent plates. There are various types of transparent material used to analyze different types of samples. For liquid samples, selected compatible IR transparent windows could be zinc selenide or diamond glasses are more appropriated. In both cases, the IR beam passes through the sample, as previously described. The low noise-to-signal ratio in samples makes the transmittance method advantageous because the pressed sample has a low number of random fluctuations of the baseline, resulting in higher sensitivity [26]. The limitations of this method include that the absorption sensitivity varies within a sample containing different thicknesses as well as the required time for sample preparation.

Transmittance FTIR has been used to monitor bacterial properties and composition in growth and non-growth [81] conditions, such as osmotic stress [13, 82], temperature shock [5, 80, 82], pH tolerance [5, 82, 95], chemical shock [5, 39, 49, 82], UV light [115], and ultra-strong static

Fig. 1 Schematic components of FTIR spectroscopy; the IR source generates radiation which passes the sample through the interferometer and reaches the detector
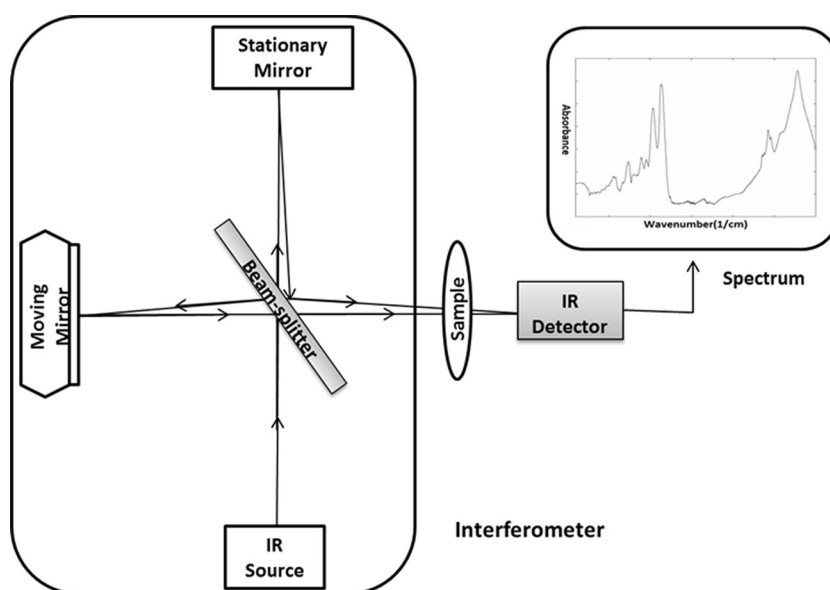
magnetic fields [50]. Likewise, the FTIR transmittance technique was used to study toxicity effects of selenium on *Escherichia coli* (*E. coli*) [39] and the exposure of *E. coli* and *Staphylococcus aureus* membrane a sequence of photocatalytic degradation followed by Ag/TiO$_2$ nanoparticle suspension [49].

Attenuated total reflectance (ATR)

For ATR–FTIR, a sample volume between 20 and 200 µL can be either directly transferred or dried and placed onto a crystal surface [16, 127] that can be made from various materials with unique refractive index relative to the sample [62]. The effective factor regarding the ATR analysis is the refractive index of the sample, which should be lower than the crystal sample holder. Depending on the type of sample, various crystal surfaces exist [16, 62, 127]. The penetration ability of the IR beam through the sample is approximately 300 nm beyond the surface of the sample. In some cases, to prevent interference from bulk water, a probe can be used to bring the IR beam directly onto the sample. A limitation of this methodology is that the resolution can decrease at higher wavelengths compared to the transmission mode due to higher background noise. However, because bacteria signatures are observed in the mid-IR, this limitation does not apply for bacteria analysis. To analyze bacterial samples by ATR–FTIR, bacteria are separated from the liquid sample by membrane filtration. Some of the types of membranes used for bacteria filtration include Metrical TM [16], polyethylene [83], Anodisc [110], and aluminum oxide [2].

ATR–FTIR has also been used to study the toxicity effect of various nanoparticles, such as ZnO [134], quantum dots [37], and carbon nanomaterial [108]. For example, Wang et al. [134] used ATR–FTIR to characterize the effect of nanowire photocatalysis on *E. coli*. Through ATR–FTIR, it was shown that structural changes occurred in the membrane composition of treated cells, indicating increased cell permeability [134]. In addition, Fang et al. [37] investigated the toxicity effect of various quantum dot nanoparticle sizes on *E. coli*. Changes in membrane structure in treated *E. coli* indicated that the toxicity effect of quantum dots depends on size, where smaller nanoparticles produce a high inhibitory effect. Likewise, Riding et al. [108] studied the toxicity effect of long and short multiwall carbon nanotubes on gram-negative bacteria. The authors reported that the bactericidal effect of carbon nanotubes depends on their size, with shorter tubes resulting in greater toxicity than longer ones based in term of revealed signature of lipids, amide II, and DNA components in treated cells.

FTIR micro-spectroscopy

FTIR micro-spectroscopy is the most recent FTIR technique and combines a FTIR spectrometer and a microscope to obtain information through the spatial and chemical spectral information simultaneously [11, 41, 62]. Sample preparation for micro-spectroscopy is performed by either drying a diluted sample directly on a IR transparent plate or pressing the IR transparent plates to a bacterial colony, which is called the "replica stamping technique" [62]. With this imprinting technique two to three bacterial layers can be placed on the plate. For both methods, the benefit is that it allows concentrating the IR radiation on the sample and collecting an accurate spectrum. It can also be applied to both the transmission and attenuated total reflection mode [41]. While micro-spectroscopy FTIR has limited spatial resolution, identifying bacteria through this accessory is not limited by this fact as they have distinct levels of morphologic heterogeneity [62].

Previous studies have reported several applications of FTIR micro-spectroscopy, including the heterogeneity during growth in *Legionella bozemanii, Bacillus megaterium,* and *Candida albicans* colonies [122] as well as *E. coli* activities in biofilms [48], endospores' bacteria changes after autoclaving [98], differences between intact and dead *E. coli* [32], live and heat-treated *Salmonella typhimurium* in chicken breast [30], the effect of membrane fluidity on resistance to high hydrostatic pressure in *Listeria monocytogenes* [55], and misfolding and aggregation changes in *E. coli* membranes in the presence of recombinant proteins [6]. FTIR micro-spectroscopy was also used to investigate the effect of a fullerene-based nanomaterial on *Bacillus subtilis* and *Pseudomonas putida* membranes [36]. The study found that the membrane fluidity and lipid composition depend on the nanomaterial concentration and the composition of the cell wall [36].

In general, the observed intensity of the absorption bands along the ATR–FTIR spectrum is less than the transmitted FTIR spectrum. The main difference between transmittance FTIR and ATR–FTIR is their depth of penetration. Transmittance FTIR measures a spectrum that is an average of the bulk properties of the sample; however, ATR–FTIR can only probe through samples up to 300 nm in thickness [16, 62, 127]. These two methods differ as well in sample preparation requirements. In the case of ATR–FTIR, the sample is directly placed on to the crystal surface, but for transmittance FTIR, the sample must be placed between two transparent glasses [16, 62, 127].

Advantages, disadvantages, and limitations

All FTIR techniques present advantages and disadvantages for the analysis of bacteria exposed to stress conditions,

such as exposure to nanoparticles. FTIR is a time-efficient technique because the sample preparation is simple [21], the time needed to obtain the spectral analysis is short [30], and samples can be analyzed in different states (liquid or solids) [17, 28, 77, 84]. In addition, only small amounts of the sample are required for analysis—usually in the order of μg (solids) or μL (liquid) [30, 78]—and the method is usually not destructive [70]. FTIR is also less expensive for bacterial identification compared to other commonly applied methods [30]. Moreover, FTIR has three remarkable advantages: (1) higher signal-to-noise ratio, (2) high energy throughput, and (3) high accuracy and stability. A higher signal-to-noise ratio is possible because the wavelengths are measured simultaneously, which is called "Fellgett advantage." Prevention of the light dispersion in FTIR causes high energy throughput which is called the "Jacquinot advantage." Regarding accuracy and stability, a remarkable advantage of FTIR is the use of a He–Ne (helium–neon) laser which acts as an internal reference for each scan and provides accurate and stable wavenumber scales of an interferometer which is referred to as the "Connes advantage." These three properties of FTIR are effective for nanotoxicology assays performed [87]. All of these three properties of FTIR are effective in the solid phase rather the liquid phase of nanotoxicological studies.

However, there are also disadvantages. Multiple background scans and sample scans are necessary to avoid artifacts and variations in the spectra due the surrounding environmental conditions in sample heterogeneity. For instance, measuring the sample in culture media at different temperatures can influence the FTIR spectra of the sample [19]. Pretreatment of the samples may be required to purify the sample and to prevent peaks from overlapping on the spectra. For example, water from bacteria samples in liquids can overlap the band of amide compounds and produce a loss of information due to the large absorption of water molecules in the 1637 cm^{-1} wavenumber [62]. In some cases, this can be avoided by preparing a dried solid sample. To identify strains of bacteria, a library for characterization and identification is required; however, this can be purchased from various scientific companies [40]. Finally, the raw data can require extensive post-processing analysis.

Additional tools to complement FTIR analysis in observing changes in intracellular composition

FTIR limitations can be compensated for by combining the analysis with other techniques. The most commonly used techniques to determine the composition of bacteria include Raman spectroscopy, mass spectrometry, nuclear magnetic resonance spectroscopy (NMR), and X-ray photoelectron spectroscopy.

Raman spectroscopy

FTIR and Raman spectroscopy have similar fundamentals as they are both inelastic scattering tools that provide a molecular fingerprint of materials based on the vibration of their molecules [59]. In Raman spectroscopy, a monochromatic light illuminates to the samples. The interactions of the impinging photons with the sample cause changes in the frequency of photons in monochromatic light. The inelastic transfer of energy then causes the frequency of the reemitted photons to shift in comparison with original monochromatic frequency. These shifts obtain information about molecular vibrational, rotational, and other low frequency transitions [27], which are called Raman effects. The elastic transfer of energy, or Rayleigh scattering, dominates the outputs of Raman spectroscopy. Therefore, in order to access Raman spectroscopy, the outputs of Raman spectroscopy require filtration by notch or band-pass filters before further analysis [27].

The main benefit of Raman spectroscopy is that it requires less sample preparation compared to some FTIR modest [27]. Although Raman spectroscopy is highly sensitive to some molecular vibrations [61], ambient noise, such as fluorescence, can interfere with the ability to obtain accurate Raman spectra [97].

Raman spectroscopy has been used to investigate the toxic effect of nanoparticle exposure to microorganisms and tracking the location of the nanoparticles with cells [60, 118]. Examples on exposure of live virus to Ag and Fe_3O nanoparticles [20], raman spectroscopy was applied to quantify the ratio of oxidized cysteine to total protein, and lipid unsaturation levels in viruses [67, 68], and to determine the location of the nanomaterial inside the microorganism [60, 118].

Raman spectroscopy has it combined with FTIR can provide valuable data about the microorganism's interactions with nanoparticles as well as nanoparticle characterization. This is possible because Raman and FTIR spectroscopies are sensitive to homo-nuclear (C–C, C=C and C≡C bonds) and hetero-nuclear (OH stretching in water) functional groups, respectively [61].

A combination of FTIR and Raman spectroscopy has been used to characterize the nanohybrid composition of silver-coated carbon nanotubes to study their antimicrobial properties [130]. Here the combined methods were used to show the successful grafting of AgNPs with amine groups onto carbon nanotubes [130].

Mass spectrometry

Mass spectrometer characterizes the mass of a molecule by determining the mass-to-charge ratio (m/z) of its ion. Ions are produced by enforcing either the loss or gain of a

charge from a sample, called the ionizing process. The ionizing process can be performed through electron bombardment, which produces the charged molecules (ions) of chemical compounds in a sample. Ions are electrostatically guided into a mass analyzer in which they are separated according to their mass-to-charge ratio and characterized. The results of molecular ionization, ion separation, and ion detection can be observed by a spectrum that provides molecular mass and structural information [63].

A specific advantage of mass spectrometry over FTIR is the capacity to quantify the structural information, although the data collected by mass spectrometry are difficult to interpret [43]. On the other hand, the analysis of compounds with multiple functional groups is very difficult when using mass spectrometry [36, 43]. Some examples of assessing toxicity effects of nanoparticles via mass spectrometry include a study focused on characterizing the interactions of bacteria with five types of nanoparticles [43]. This study determined the preferential binds between peptide fragments and surface coating of silver nanoparticles [126] and quantified the formation of oxidatively induced DNA lesions in different types of cells exposed to gold nanoparticles [90].

Mass spectrometry and FTIR are tools that are often used in conjunction; FTIR provides an outlook into the structural overview of bacterial toxicity, whereas mass spectrometry offers a ratio of molecular bonds [36]. For example, Fang et al. [36] investigated the impact of buckminsterfullerene (C_{60}) on membrane properties on gram-positive and gram-negative bacteria. In this study, FTIR showed that the frequency of $-CH_2$ stretching increased due to the high concentration of nanomaterials, which means the fluidity of the membrane was increased in treated cells. Mass spectrometry also showed that the proportions of monounsaturated fatty acids in treated bacteria increased significantly compared to the controls [36].

Nuclear magnetic resonance spectroscopy (NMR)

NMR characterizes the physical and chemical properties of certain atomic nuclei. As all electrically charged nuclei have an associated spin, the applied external magnetic fields transfer energy at a specific wavelength from the base energy to a higher energy level. The wavelength corresponds to radio frequencies; hence, when the spin returns to its base level, energy is emitted at the same frequency, and the released signal results in an NMR spectrum for the nucleus [117].

NMR spectroscopy can determine the molecular structure, content, and purity of a sample. NMR can detect an unknown compound's molecular structure and match it against spectral libraries or directly infer them from basic structures of molecules [116]. In the case of known compounds, NMR can characterize the molecular structure as well as physical properties at the molecular level. These properties include structural changes, phase changes, solubility, and diffusibility [116].

In order to analyze more complex materials such as bacteria [116], NMR is more appropriate than the previously mentioned techniques. Some advantages of this tool are versatile identification in terms of material composition and high chemical sensitivity [117]. NMR can measure the long-range hetero-nuclear distances, which can be used to measure a distance between an antibiotic and a specific site in the membrane [22]. In addition, NMR can determine protein structures and the location of every atom in the space [113]. One of the disadvantages is that NMR has the potential to change the genetic code of bacteria and consequently the behavior of the protein, due to the use of synthesized amino acids for labeling [105].

Several studies have used NMR to measure the effectiveness of antimicrobial agents on intact *E. coli* without mutation or on mutated strains deficient in total fatty acid biosynthesis [31, 101, 121], as well as study the adaptation mechanisms of bacteria to peptides [23], or detect peptidoglycan composition and define the interactions with *S. aureus* [111].

The combined NMR and FTIR approach was applied to investigate the interaction of different structures of peptides (α-helices and β-sheets) with the bacterial membrane and its diastereomer [94]. NMR revealed the interactions between peptides within membranes, while FTIR characterized the composition of α-helical structures within the peptide. NMR also detected the ratio of α-helical and β-sheets within membranes. The combined approach showed which peptide organized more selectively with the membrane [94].

To our knowledge, no study has used NMR and FTIR combined for nanotoxicology. However, NMR as well as FTIR supports the identification of functional groups' alterations in bacteria [31, 101, 121]. A spectrometric analysis of bacteria exposed to nanoparticles by NMR can provide comprehensive information about the molecular composition of cells and complement the FTIR results.

X-ray photoelectron spectroscopy (XPS)

In XPS, photoelectrons are emitted from the sample surface due to excitation with monoenergetic Al kα X-rays. The energy of emitted photoelectrons is measured by an electron energy analyzer. The photoelectron peak determines the binding energy and intensity of the elemental identity, chemical state, and quantity of an element. XPS has different detection limits and analysis depths to detect the chemical composition of different cells [10, 15, 33, 34, 92, 93, 103, 112, 124, 128].

XPS determines the presence of elements and the composition of functional groups, such as proteins and polymeric substances on the cell surface [10, 15, 33, 34, 92, 93, 103, 112, 124, 128]. XPS can also estimate the concentrations of the bacterial surface compounds within 5 nm from the sample surface [1, 46, 92]. These include functional group identification of polysaccharides, peptides, and hydrocarbon compounds with the use of a constituent model [1, 34, 104]. XPS has been used to identify the accurate composition of polymer surfaces and their adhered biomolecules [123] as well as to study cell–substratum interfaces [14]. Moreover, XPS identified the gram-negative *Aquabacterium* surface properties, including surface charge, acid–base behavior, chemical composition, and changes in the organic functional groups at different pH values [92].

The main limitation of XPS is the effective depth of the cell surface, which limits the application of this technique to extracellular analysis [120]. This technique can provide the quantitative elemental analysis of all elements, except hydrogen and helium, both of them which are generally free of matrix effects and decrease quantitative accuracy [10, 33, 34, 92, 93, 103, 112, 128]. Other disadvantages of this technique are that hydrogen cannot be detected by XPS and the requirement for a high vacuum, which results in a slow characterization process (8 h). Finally, the deconvolution of XPS peaks should be carried out with extreme care because these peaks are notorious for leading to spurious results [120]. Even though these limitations are present, this technique is useful analyzing bacterial surface interactions because of quantitative measurement and chemical bond identification based on elemental characterization [46, 64].

In terms of studying toxicity effects, XPS has been applied to characterize the nanoparticle surface properties, such as characterizing the surface coating of Ag–TiO$_2$ nanoparticles and then complementing this analysis by studying the bactericidal effect of these nanoparticles via FTIR [72].

Bacteria–nanoparticles interactions at the molecular level measured by FTIR

Several possible antimicrobial mechanisms have been detected using FTIR: (1) nanoparticles may change the fluidity of cell wall lipids by binding with –CH groups of the membrane [36, 49, 58, 86] measured at 3100–2800 cm^{-1}; (2) the binding of nanoparticles, or ions released from nanoparticles, with amino acids in proteins and enzymes [35], which changes the protein structures detectable at 1500–1800 cm^{-1} [16]; (3) nanoparticles bound to phosphate groups of nucleic acids in DNA or

RNA altering their structures, which are detected in the 600–1200 cm^{-1} wavenumber range [35, 52]; and (4) nanoparticle catalyzed oxidation mechanisms and generation of reactive oxygen species (ROS) [35], which can cause alterations in polysaccharide structures measured in the 900–1200 cm^{-1} wavenumber [52] range. The chemical properties of bacteria exposed to nanoparticles can be determined from previous studies that introduced the specificity of the altered chemical groups [36, 37, 49, 52, 58, 86, 108, 134]. As previously mentioned, FTIR is able to reveal different biochemical properties of bacteria based on their chemical bonds [1–12] and structural changes [131]. The biochemical structural alterations of bacteria exposed to nanoparticles can be characterized in four regions by tracking FTIR fingerprints [36, 37, 49, 52, 58, 86, 108, 134]. These regions are mainly placed between 3100 and 2800 cm^{-1} for fatty acids, 1800 and 1500 cm^{-1} for proteins and peptides, 1200 and 900 cm^{-1} for carbohydrates, and 900 and 600 cm^{-1} for the fingerprint region [62]. The impacts of nanoparticles in each of these regions are described below.

Fatty acid region

The chains of several bacterial membrane amphiphiles (e. g., phospholipids) and side-chain vibrations can be characterized by the peaks in the region around 3100–2800 cm^{-1}, which are observed due to the –CH stretching vibrations of CH$_3$, CH$_2$, and CH functional groups [62, 89]. The bands in 2955, 2930, 2898, 2870, and 2850 cm^{-1} wavenumbers are responsible for –CH asymmetric stretching of –CH$_3$ in fatty acids, –CH asymmetric stretching of >CH$_3$ in fatty acids, –CH stretching of ≥–CH of amino acids in fatty acids, –CH symmetric stretching of –CH in fatty acids, and –CH symmetric stretching of CH$_2$ in fatty acids, respectively [62]. Sometimes a peak at 3015 cm^{-1} was reported as a responsible band for stretching CH double bonds in unsaturated fatty acid chains [62].

Fatty acids' spectral bands between 3100 and 2800 cm^{-1} [85, 119] can determine the severity of the nanoparticles' impact on the bacterial wall. The resolved peaks in the majority of published articles characterized the differences between bacterial fatty acids' profiles in the presence of nanoparticles and untreated bacteria [36, 37, 49, 58, 86, 134]. Membrane peroxidation in *E. coli*-exposed TiO$_2$ photocatalysis was detected through modifications of bands at 2958, 2924, 2876, and 2854 cm^{-1}, which were caused by –CH asymmetric stretching of –CH$_3$ in fatty acids, –CH asymmetric stretching of >CH$_3$ in fatty acids, and –CH symmetric stretching of CH$_2$ in fatty bands [58, 86]. Similarly, Hu et al. [49] reported that the main alteration in the fatty acid region included reduced peak intensity of the

–CH bands at 2872 and 2852 cm^{-1} as well as undetectable bands at 2963 and 2927 cm^{-1} in bacteria exposed to AgI/TiO$_2$ nanoparticles for 6 h. Also, Fang et al. [37] observed changes after exposing *E. coli* to different sizes of the CdTe quantum dot nanoparticles. They characterized the intensity of bands at 2958, 2925, and 2854 cm^{-1} and found that peaks were smaller in treated bacteria compared to the control. The authors reported that the alterations in –CH of the fatty-tail structure are the cause of smaller peak intensity at these wavenumbers. Furthermore, they found that the –CH band at 2873 cm^{-1} disappeared after treating bacteria with the small size of CdTe quantum dots. Another study detected that the effects of the ZnO nanowire photocatalysis were characterized in the fatty acid regions by the decreased bands at 2852, 2924, and 2959 cm^{-1}, indicating the changes in –CH of the fatty-tail structure [134]. Moreover, other studies focusing on bacteria treated with different concentrations of fullerene-based nanomaterials reported that a decreasing intensity ratio of CH$_2$ vibration indicates the alteration of membrane fluidity [36]. A modification of the –CH vibration on the exposed bacterial profile is interpreted as bacterial lysis [36, 37, 49, 58, 86, 134], thereby indicating an increase in the lipid-layer fluidity of the bacterial cell walls. The enhanced fluidity of the lipopolysaccharides cause a leakage in the cell membrane [74] that has been reported due to the peroxidation in the case of polar-saccharide moieties [88].

Additional information for the fatty acid region can be derived from the responsible bands for –CH deformation in the 1500–1200 cm^{-1} area [12, 30, 62]. The bands around 1367, 1354, and 1341 cm^{-1} are responsible for the vibrations of methylene fragments in the kink (gauche-*trans*-gauche), double-gauche, and end-gauche conformations, respectively [25, 66]. After bacterial exposure to oxide nanoparticles, the band at 1341 cm^{-1} disappeared and intensive bands at 1362 cm^{-1} were observed [52], indicating a low concentration of the vibrations of methylene in end-gauche conformers as well as a combination of vibrations of methylene in gauche-*trans*-gauche and double-gauche conformers, respectively [25, 66]. Hu et al. [49] reported that the increase in the concentration of carboxylic groups was due to the appearance of bands at 1408 and 1337 cm^{-1}. They concluded that the photocatalytic degradation of the cell membrane causes the formation of carboxylic acid. In addition, some spectral changes were reported near 1414 and 1390 cm^{-1}, indicating the unsaturated aldehydes due to the deformation of the hydroperoxides or lipid endoperoxides and the appearance of C=O stretching bonds [42].

In the case of characterizing alterations in the phospholipids of nanoparticle-exposed bacteria, bands for the PO^{-2} asymmetric stretching of phosphodiesters in phospholipids should be detected near 1280–1200 cm^{-1}. Based on various studies, phosphate groups on the FTIR spectra demonstrated the decrease in peak intensity around 1232 cm^{-1} [37] or 1234 cm^{-1} [134] bands due to the sensitivity of the hydration–dehydration of the phosphoric groups in lipids structures [30, 57]. This mechanism is responsible for the change in permeation in terms of the depletion in ATP levels [35] that has been reported as a nanoparticles' impact on bacteria [36, 37, 49, 58, 86, 134]. Moreover, Riding et al. [108] claimed that the decreased peak at 1238 cm^{-1} in the carbon nanotube-treated bacteria indicated the inhibition of releasing free ROS.

Moreover, other wavenumber regions were reported for phospholipid and phosphodiester compounds. For instance, a decreased intensity of peaks was reported for phospholipid and phosphodiester compounds around 1080 cm^{-1}, suggesting the peroxidation of the hydrophobic end [134]. They also reported the appearance of two bands at 1111 and 976 cm^{-1} after ZnO nanoparticle exposure, which introduced a signature of the symmetry and asymmetric vibration of deprotonated PO$_3^{2-}$, suggesting that part of the PO^{2-} groups in phosphodiester was converted into terminal phosphoryl PO$_3^{2-}$ groups. In addition, a new band formed at 937 cm^{-1} after exposure to ZnO nanoparticles might relate to the symmetry vibration of PO$_4^{3-}$ [51, 99]. This band may appear from the deviation of terminal phosphoryl groups caused by the CH$_2$ wagging spectra.

The destruction of polar saccharides as a result of ROS generation by nanoparticles caused clear changes in the wavenumbers in the fatty acid region of treated bacteria compared to untreated cell spectra [36, 37, 49, 58, 73, 86, 134].

Protein region

The peaks at 3200 and 3060 cm^{-1} indicate N–H stretching of amide A and amide B, respectively, in proteins [13, 39, 89, 115]. Furthermore, the majority of responsible peaks for the protein region mainly include the peaks at 1800 and 1500 cm^{-1}, which are dominated by the amide I and amide II of proteins and peptides, except the amide III band, which is located around 1280 cm^{-1}. The amide I band components of proteins rise near the 1695–1675 cm^{-1} area. Certain peaks at 1655 and 1637 cm^{-1} are responsible for the rise in amide I principally due to the stretching vibrations of the C=O groups at α-helical and β-pleated sheet structures of proteins, respectively. Amide II bands of proteins show up in the 1550–1520 cm^{-1} region due to N–H bending with contributions from the C–N stretching vibrations of the peptide group. As previous reports have mentioned, amide I and amide II bands present the predominance of α or β structures [11, 62]. Amino acids can also be detected by FTIR; for instance, tyrosine can be detected by the peak in 1515 cm^{-1} [11, 62, 75, 89, 129].

Other amino acids such as aspartate and glutamate demonstrated weak peaks between 1585 and 1570 cm^{-1} due to the stretching vibration of carboxylate groups [62].

Interactions between metal nanoparticles and thiol groups of respiratory chain enzymes and other amino acid groups of bacterial membranes [38, 69] yield to the thought of FTIR's affordability for detecting the alterations of protein conformation in nanoparticle-treated bacteria. The altered peaks caused by protein structural changes were reported in several articles and characterized the differences between the bacterial protein profiles in the presence of nanoparticles and untreated bacteria [36, 37, 49, 58, 86, 108, 134]. The spectral profile resulting from bacteria exposed to different sizes of nanotubes based on FTIR analysis indicated the alteration of bands at 1497 and 1485 cm^{-1}, which were introduced as dominant protein conformational alterations [108]. Similarly, the decrease in peak intensity was reported at 1639 and at 1539 cm^{-1}. The authors further claimed a decreased intensity of the amide A band at 3290 cm^{-1} due to the conformational changes in amide groups at the hydrophobic end of the phosphor lipids [134]. In addition, Hu et al. [49] found a decrease in peak intensity of bands near 1653 and 1545 cm^{-1} after exposing pathogenic bacteria to AgI/TiO$_2$ nanoparticles under visible light irradiation, which indicates that increasing exposure time causes the decrease in the concentrations of amide I and amide II groups [49].

Fang et al. reported protein conformational changes in treated gram-negative bacteria exposed to quantum dot nanoparticles [21]. Here, clear decreases in peak intensity were observed after exposure in the spectral peaks at 1645, 1540, and 3288 cm^{-1}. In another study, where gram-positive bacteria were exposed to oxide nanoparticles, the bands at 1600 and 1408 cm^{-1} showed increases in peak intensity compared to the control [15]. A possible explanation for the mechanism in the gram-positive bacteria exposed to oxide nanoparticles is that the carboxyl group concentrations increased due to the contribution of the carboxylic groups forming an inner sphere complex with the oxide metal center. Another explanation is that the ester bond of D-alanine branch is connected to the exposed gram-positive bacteria and then detached to form D-alanine acid [93]. Upon the gram-positive bacteria exposure to oxide nanoparticles, the intensity ratio of β-sheets to α-helices also decreased [4]. This can be explained by lower sensitivity of the FTIR to detect hydrogen-bonding carbonyl groups which changed the β-sheet structure; alternatively, the β-sheet intensity of the protein may have been diminished due to unfolding [53] after interaction with nanoparticles.

Changes in the protein region, such as peaks at 1414 cm^{-1}, as reported by Nadtochenko et al., include the C–O–H in-plane bending of carbohydrates, DNA/RNA backbone, and proteins [58, 86]. Also, bands at 1390 cm^{-1} may be influenced by the effect of nanoparticles on bacteria due to the C=O symmetric stretching of COO– group in amino acids and fatty acids. Some spectral changes have been reported, corresponding to the formation of the α and β structures of unsaturated aldehydes because of the breakdown process of hydroperoxides or lipid endoperoxides [42]. Finally, in another study, changes in the peaks at 1390 cm^{-1} derived a possible explanation based on the presence of nitrocompounds from proteins or enzymes during the bacterial protection mechanisms. These compounds corresponded to the nanoparticle-exposed bacterial resistance mechanisms to decrease the effect of nitrosative stress at the transcriptional level [96].

The results of the discussed report clarified that the peptide and amino acids, regardless of their position (intracellular or extracellular), were modified in the nanoparticle-treated bacterial FTIR signature.

Carbohydrates region

The spectral changes after bacteria exposure to nanoparticles may take place in the 900–1200 cm^{-1} area, which is dominated by C–O–C and C–O ring vibrations in various polysaccharides. In detail, the region of 1120–1140 cm^{-1} relates to the v(C–O–C) glycosidic linkage [79] and peaks around 1153, 1117, 1102, 1058, 993, and 966 cm^{-1}, corresponding to the v(C–O) ring, v(C–O), v(C–C), and δ(COH) vibrations of carbohydrates [54].

The profiles of polysaccharide bands after treatment with nanoparticles have been reported with obvious changes [52, 86, 134]. The bands at 1117 and 1102 cm^{-1} disappeared in the asymmetric vibration of the C–O–C glycosidic linkage regions, respectively, and a new band showed up at 1120 cm^{-1}. Also a decrease in intensity of the broad 1140–1000 cm^{-1} band was detected. These spectral changes to lipopolysaccharides peroxidation can be explained by the composition of the asymmetric outer membrane, amphipathic molecules, or lipopolysaccharides [54, 88]. Another study reported a decrease in peak intensity at 1188 cm^{-1} that corresponds to carbohydrate changes, indicating the occurrence of ROS-induced damage [108]. Jiang et al. [52] reported in a different study that after exposing bacteria to ZnO nanoparticles, the sugar bands at 1074 cm^{-1} shifted to a lower wavenumber, suggesting the weakening of the C–O bond due to an increase in the degree of strength of hydrogen bonding with oxides.

The negative surface charge of bacteria due to polysaccharides of lipopolysaccharides provides interaction with the positively charged nanoparticles and forms pit structures in the membrane [109]. These pit structures could be detected by FTIR in the polysaccharides region because they are formed by disrupting the β-1 → 4 glycosidic bonds of the membrane [35].

Fingerprint region

The fingerprint falls between wavenumbers 900–600 cm^{-1} and indicates unique weak bands that correspond to nucleic acids, i.e., phenylalanine, tyrosine, tryptophan, and various nucleotides [62]. The discrimination of bacteria at the strain level can be performed in the fingerprint region [30]. Bands corresponding to bacterial nucleic acids are not limited to the fingerprint region; two peaks can be observed around 1715 and 1415 cm^{-1} which are responsible for >C=O stretching of esters in nucleic acids and carbonic acids and C–O–H in-plane bending in the DNA/RNA backbone [62].

In bacteria treated with nanoparticles, an increased band near 1738 cm^{-1} was observed due to vibration of the C=O carbonyl group. The possible explanation is the peroxidation of nucleic acid chains (Zeroual et al 1994) because of oxidative stress by the generation of ROS [35, 49, 52]. Hu et al. [49] provided an explanation for the increased peaks at 1690 and 1734 cm^{-1} in exposed bacteria, which indicate an increase in concentration of C=O bonds in aldehydes and ketones. Additionally, due to a pH change in bacteria exposed to nanoparticles, the functional groups of the nucleic acid also undergo changes, which can be revealed in the fingerprint region of the FTIR spectra [18].

Example of ATR–FTIR use for the study of *E. coli* exposure to AgNPs using batch reactors

Escherichia coli K-12 (ATCC 23716), a non-pathogenic strain, was selected for this study. *E. coli* is a gram-negative bacterium that has been found to be metabolically active and has been extensively studied in nanotoxicological research [7, 114, 133]. Reagent used to prepare the lysogeny broth (LB) Miller growth media consisted of 10 g/L NaCl, 5 g/L yeast extract, and 10 g/L tryptone [106] which it was based on ATCC recommendations. The bacteria were stored in phosphate buffer solution (PBS)—monobasic potassium phosphate, dibasic potassium phosphate, and Ethylenediaminetetraacetic acid (EDTA)—which were all purchased from Sigma-Aldrich. Standard casein-coated silver nanoparticles (AgNPs) were obtained from the Argenol Company, Spain.

Micro-plates with six wells were used to grow bacteria until log phase, measuring the optical density at 600 nm (OD600) every 15 min. After 7.5 h of bacterial growth, suspensions of AgNPs in deionized water were injected to achieve a concentration of 15 mg/L inside of the exposed condition (media plus bacteria + AgNPs). Controls wells were included to detect contamination (media with no bacteria), and comparison between the non-exposed condition (media plus bacteria) and exposed condition. After

that, plates were run for 7.5 additional hours to assess AgNPs toxicity at 2.5, 5, and 7.5 h.

Liquid samples were prepared for ATR–FTIR (Nicolet iS50 FTIR, Thermo Scientific) analysis by fixing the optical density (OD600) to 0.8 using a UV–Vis spectrophotometer (Genesis, 10UV, Thermo Scientific). Following this, bacteria were centrifuged at 13,000 rpm for 10 min, and the supernatant was removed. The pellets were suspended in 10 μL of PBS 10 % [132], and the suspension of bacteria with AgNPs was directly placed onto the crystal surface [45].

Spectra were the result of 256 scans with a resolution of 4 cm^{-1} in the 4000–350 cm^{-1} spectral range. The data were provided by Omnic software (Thermo Scientific) and processed using MATLAB (MathWorks Software).

A unique FTIR spectrum is detected for the AgNP treated bacteria after each contact time (Fig. 2). Increased contact time resulted in decreased peaks in the spectra, where the untreated bacteria had the most intense peaks throughout the spectrum compared to the bacteria exposed for 7.5 h, which had the weakest intensity peaks. To detect the specific responses within the treated bacteria, the data were analyzed region by region on the spectra.

Figure 3 shows the spectra for the fatty acid region, including the *E. coli* profile and *E. coli* exposed to AgNPs. The obvious changes were related to shifting due to the deformation of >CH$_2$ and v_s(C=O) in lipids after 7.5 h of treatment (Table 1). The change in the asymmetry vibration of phosphate groups also disappeared after 7.5 h of exposure. The observed changes in the fatty acid region can be due to the alterations in the fluidity of the cytoplasm membrane or cell wall.

Figure 4 shows the ATR–FTIR spectra in the 1800–1200 cm^{-1} range of the *E. coli* as a control and *E. coli* exposed to AgNPs. The ATR–FTIR protein region peaks of *E. coli* before and after treatment are shown in (Table 2).
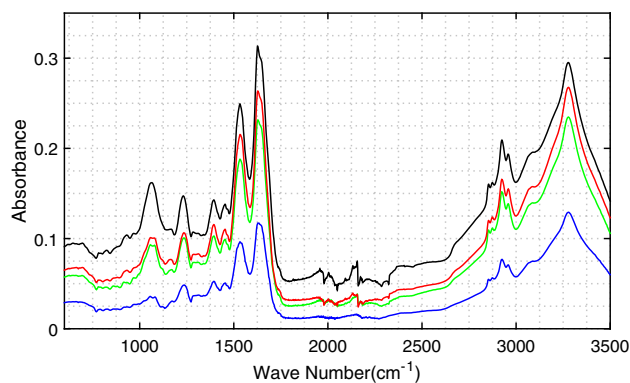
Fig. 2 ATR–FTIR spectra region in untreated *E. coli* (*black line*), *E. coli* + AgNPs after 2.5 h (*red line*), *E. coli* + AgNPs after 5 h (*green line*), and *E. coli* + AgNPs after 7.5 h (*blue line*) (color figure online)
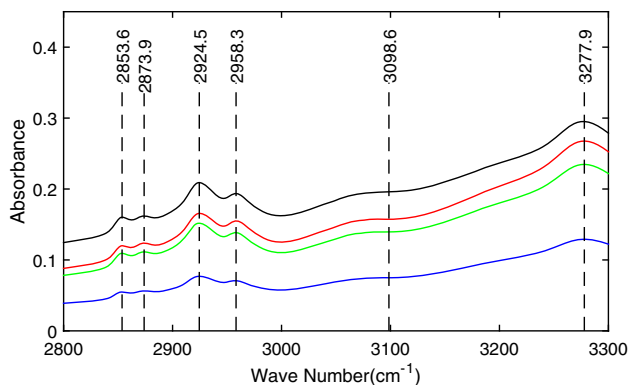
Fig. 3 ATR–FTIR spectra of fatty acid region in untreated *E. coli* (*black line*), *E. coli* + AgNPs after 2.5 h (*red line*), *E. coli* + AgNPs after 5 h (*green line*), and *E. coli* + AgNPs after 7.5 h (*blue line*) (color figure online)

The band at 1284.8 cm^{-1} showed increased peak intensity in order to express the presence of amide III components of proteins in untreated *E. coli*. This band was shifted to 1287.3 cm^{-1} after 2.5 and 5 h of exposure, but disappeared after 7.5 h of exposure. Furthermore, amide A and amide B bands were observed at 3098.6 and 3277.9 cm^{-1} in the untreated bacterial profile, respectively. However, the greatest shifting happened for the amide B band after 2.5 h of treatment and remained consistent until 7.5 h of treatment (Fig. 3; Table 2).

Bands between 1200 and 900 cm^{-1} showed the presence of C–O–C and C–O vibrations in the sugar rings in various components of polysaccharides (Fig. 5a). The peaks at 1167.7, 1145, 968.1, and 932.4 cm^{-1} were observed in the untreated *E. coli* spectra. However, after 2.5 h of exposure to nanoparticles, the peaks appeared in different wavenumbers, such as 1163, 1058.4, and 932.4 cm^{-1}. The band responsible for v(C–C) was observed at 1058 cm^{-1} in the spectra after 2.5 h of exposure. This band was shifted to 1057.3 after 5 h of treatment time and did not exist in

untreated *E. coli*. A major shift was seen because of the v(C–O) ring for *E. coli* from 1167.7 to 1163 cm^{-1} after 2.5 h of exposure and again to 1169.3 cm^{-1} after 5 h. Despite the fact that the band at 932.4 cm^{-1} was shifted to 916.5 cm^{-1} after 5 h of exposure, this band did not change after only 2.5 h of exposure. In addition, a band at 968.6 cm^{-1} appeared in the spectra of untreated *E. coli* and exposed *E. coli* after 5 h, while the exposed *E. coli* after 2.5 h did not exhibit this band. All peaks of this region disappeared after 7.5 h of nanoparticle exposure. The deformation of bacterial cell walls can be the reason of the shifting in the carbohydrate region (Fig. 5a), which shows P=O symmetric stretching in DNA, RNA, and phospholipids bands that shifted from 1064 cm^{-1} in untreated *E. coli* to 1078 cm^{-1} after 2.5 and 5 h of exposure.

In the region between 900 and 600 cm^{-1}, weak bands appeared (Fig. 5b). The fingerprint bands of *E. coli* are 824.9, 782, 665.8, and 620 cm^{-1}, which shifted to 827.8, 781.5, 661.9, and 624.3 cm^{-1}, respectively, after 2.5 h of treatment. Changes were observed in exposed *E. coli* spectra after 5 h and appeared in the spectrum of treated bacteria at 693.3, 643.6, and 623.4 cm^{-1}. All peaks in the fingerprint region disappeared after 7.5 h of treatment.

Some specific peaks showed unique behavior in the fingerprint region. The peak at 644.1 cm^{-1} only appeared in untreated samples and was not seen in any of the treated samples. On the contrary, a band at 881.8 cm^{-1} appeared at 2.5 h, which was not present in the untreated bacteria, nor did it appear in the 5 h sample. In contrast, the band at 695.2 cm^{-1} was not changed at all after exposure. The reason for the changes in this region may be due to the alteration of the secondary and tertiary helix structure of DNA, the generation of new gene fragments, or an increase in the transcriptional in the DNA molecule [50].

The results showed that the spectral regions changed based on the time of exposure after treatment of bacteria with nanoparticles. The results indicated that 7.5 h showed

Table 1 Comparison of fatty acids region of untreated *E. coli* and treated *E. coli* with AgNPs at 0, 2.5, 5, and 7.5 h of treatment using ATR–FTIR

Vibration mode	*E. coli* Wavenumber (cm^{-1})	*E. coli* + AgNPs (2.5 h) Wavenumber (cm^{-1})	*E. coli* + AgNPs (5 h) Wavenumber (cm^{-1})	*E. coli* + AgNPs (7.5 h) Wavenumber (cm^{-1})
v_a(CH$_3$)	2958.3	2958.3	2957.8	2957.3[a]
v_a(CH$_2$)	2924.5	2924.5	2924.5	2924.5
v_s(CH$_3$)	2873.9	2873.9	2873.9	2873.9
v_s(CH$_2$)	2853.6	2853.6	2853.6	2853.2
>CH$_2$ deformation	1453.6	1453.6	1453.6	1454.1[a]
v_s(C=O)	1393.8	1393.8	1393.8	1394.3
v_a(P=O)	1235.2	1235.2	1235.2	–[b]

[a] Peak was shifted to a different wavenumber

[b] Peak was not observed
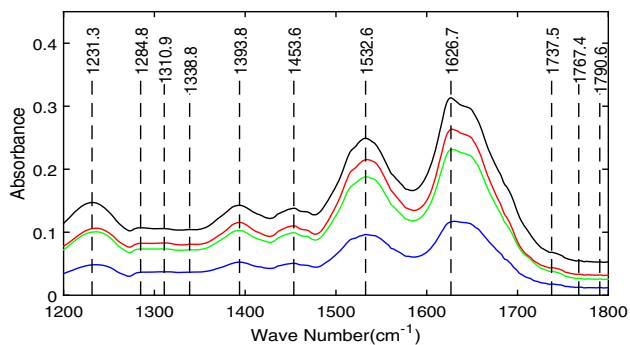
Fig. 4 ATR–FTIR spectra of 1200–1800 cm^{-1} region of untreated *E. coli* (*black line*), *E. coli* + AgNPs after 2.5 h (*red line*), *E. coli* + AgNPs after 5 h (*green line*), and *E. coli* + AgNPs after 7.5 h (*blue line*) (color figure online)

the most spectral modifications. The most remarkable differences were found in the peptide and amino acids region. This could suggest that part of the ATR–FTIR spectral changes were due to the damage of conformational/compositional alterations in some of the components of the

protein structures that could be intracellular proteins or cell wall peptides [52, 58]. While the majority of previous studies have focused on membrane alterations [36, 49, 58, 86, 134], Jiang et al. [52] also reported modifications in the different bacterial strains of protein structures after being exposed to oxide nanoparticles. Even though the reference study used oxide nanoparticles [52], the mechanism for modifications in bacterial protein structures may be similar to the toxicity effect observed here. The cytotoxicity effect of oxide nanoparticles onto bacteria was also shown in the proteins region of the bacterial profile. The changes in the intensity ratio of β-sheets/α-helices were reported as a protein structure alteration [52].

The interactions of AgNPs that caused the changes in the fatty acids, specifically –CH deformation, can be the reason for alteration in membrane permeability, which suggests the formation of pits in the bacterial cell wall. Another reason for differences in membrane permeability is the modification at the cellular ATP level, which was observed in exposed bacterial spectra due to the

Table 2 Comparison of proteins region of untreated *E. coli* and treated *E. coli* with AgNPs at 0, 2.5, 5, and 7.5 h of treatment using ATR–FTIR

Vibration mode	*E. coli* Wavenumber (cm^{-1})	*E. coli* + AgNPs (2.5 h) Wavenumber (cm^{-1})	*E. coli* + AgNPs (5 h) Wavenumber (cm^{-1})	*E. coli* + AgNPs (7.5 h) Wavenumber (cm^{-1})
Amid A	3277.9	3277.9	3277.9	3277.9
Amid B	3098.6	3088.9*	3089.4*	3089.4[a]
Amid I	1626.7	1627.6	1627.6	1628.1[a]
Amid II	1532.6	1533.1	1533.1	1532.6[a]
Amide III	1284.8	1287.3	1287.3	–[b]

[a] Peak was shifted to a different wavenumber

[b] Peak was not observed
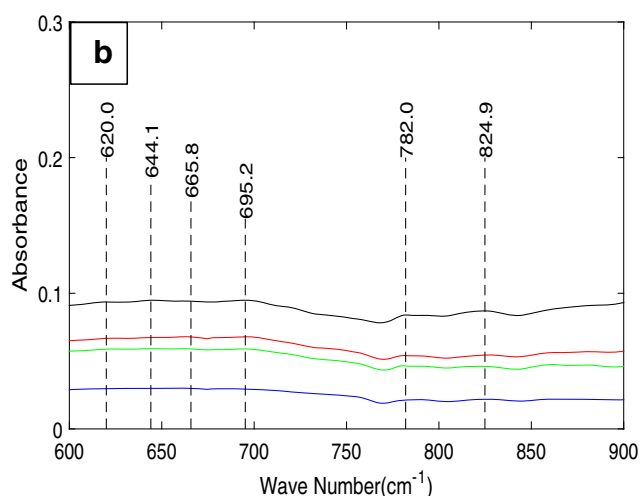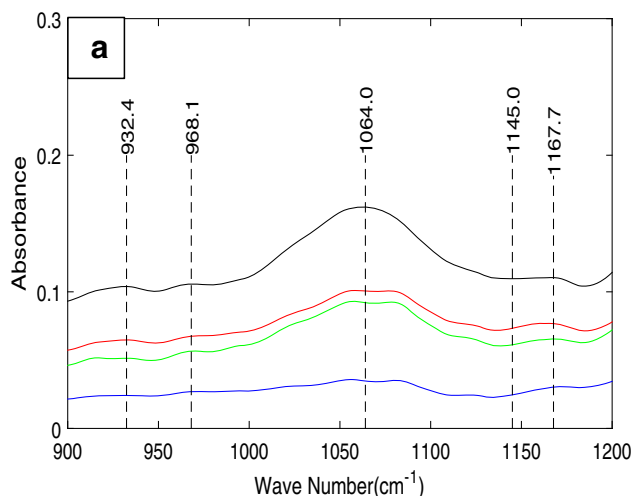
Fig. 5 a ATR–FTIR spectra of 900–1200 cm^{-1} and **b** ATR–FTIR spectra of 900–600 cm^{-1} region of untreated *E. coli* (*black line*), *E. coli* + AgNPs after 2.5 h (*red line*), *E. coli* + AgNPs after 5 h (*green line*), and *E. coli* + AgNPs after 7.5 h (*blue line*) (color figure online)

dehydration of phospholipids. In another study where bacteria were exposed to ZnO nanoparticles, the phosphodiester bond was modified in treated cells and formed phosphate monoesters [52]. This resulted in highly disordered alkyl chains yielding membrane ruptures and cell leaking [52]. The deformation of the fatty acid can be derived from the presence of unsaturated aldehydes during the deformation of hydroperoxides or lipid endoperoxides and the appearance of P=O stretching bands. Other studies also reported the shifting of fatty acids bands due to the toxicity effect of oxide nanoparticles [58, 86]. These impacts on phosphate groups' stretching may be caused by the ROS, which identify malfunctions in the respiratory chain enzymes and other membrane proteins and lipophospho-polysaccharids [52].

This study shows that AgNPs can impact the structure and function of proteins [74, 109, 126] and can damage nucleic acid molecules [24, 44]. The effect of membrane alterations in the treated bacteria was less compared to the observed changes in proteins. Furthermore, slight changes in membrane permeation were detected using epifluorescence stains and extracted lipid monolayers of *E coli* exposed to AgNPs after 5 h (Anaya et al.). However, even these small changes were enough to damage the outer cell membrane by AgNPs, which causes more entry of AgNPs into the cells could be one of the reasons that AgNPs have cytotoxic effect on *E. coli* [9, 126, 133] while another reason could be that a decrease in ATP levels inside the bacteria occurs due to the lack of nutrients and oxygen after 7.5 h in a batch growth system.

Conclusion

FTIR is an extremely rapid technique compared to conventional techniques. FTIR has uniform applicability to various bacteria and a high specificity for differentiating toxic effects at intracellular levels. Thus, it can provide clear discrimination between chemically exposed bacteria in comparison to controls. The spectral range in this method could assist in rapidly evaluating the toxicity level of different stressors, such as nanoparticles. Consequently, FTIR spectroscopy could be successfully applied to characterize time-dependent toxicity impacts of nanoparticles in bacteria and to assess the intensity of cell sensitivity toward physical or chemical treatments. FTIR techniques in this context provide diagnostic methods for different forms of samples. Complementary techniques, such as NMR, Raman, XPS, and mass spectroscopy, can increase the information density in order to determine the intracellular composition and structures of treated and untreated cells.

References

1. Ahimou F, Boonaert CJP, Adriaensen Y et al (2007) XPS analysis of chemical functions at the surface of *Bacillus subtilis*. J Colloid Interface Sci 309:49–55. doi:10.1016/j.jcis.2007.01.055
2. Al-Holy MA, Lin M, Cavinato AG, Rasco BA (2006) The use of Fourier transform infrared spectroscopy to differentiate *Escherichia coli* O157:H7 from other bacteria inoculated into apple juice. Food Microbiol 23:162–168. doi:10.1016/j.fm.2005.01.017
3. Al-Qadiri HM, Al-Alami NI, Al-Holy MA, Rasco BA (2008) Using Fourier transform infrared (FT-IR) absorbance spectroscopy and multivariate analysis to study the effect of chlorine-induced bacterial injury in water. J Agric Food Chem 56:8992–8997. doi:10.1021/jf801604p
4. Al-Qadiri HM, Lin M, Al-Holy MA et al (2008) Detection of sublethal thermal injury in salmonella enterica serotype Typhimurium and *Listeria monocytogenes* using Fourier transform infrared (FT-IR) spectroscopy (4000 to 600 cm^{-1}). J Food Sci 73:M54–M61. doi:10.1111/j.1750-3841.2007.00640.x
5. Alvarez-Ordóñez A, Halisch J, Prieto M (2010) Changes in Fourier transform infrared spectra of Salmonella enterica serovars Typhimurium and Enteritidis after adaptation to stressful growth conditions. Int J Food Microbiol 142:97–105. doi:10.1016/j.ijfoodmicro.2010.06.008
6. Ami D, Natalello A, Schultz T et al (2009) Effects of recombinant protein misfolding and aggregation on bacterial membranes. Biochim Biophys Acta BBA Proteins Proteomics 1794:263–269. doi:10.1016/j.bbapap.2008.10.015
7. Anaya NM, Solomon F, Oyanedel-Craver V (2015) Effects of dysprosium oxide nanoparticles on *Escherichia coli*. Environ Sci Nano. doi:10.1039/C5EN00074B
8. Anaya NM, Faghihzadeh F, Ganji N et al (2016) Comparative study between chemostat and batch reactors to quantify membrane permeability changes on bacteria exposed to silver nanoparticles. Sci Total Environ. doi:10.1016/j.scitotenv.2016.03.039
9. Arora S, Jain J, Rajwade JM, Paknikar KM (2008) Cellular responses induced by silver nanoparticles: in vitro studies. Toxicol Lett 179:93–100. doi:10.1016/j.toxlet.2008.04.009
10. Beech IB, Zinkevich V, Tapper R et al (1999) Study of the interaction of sulphate-reducing bacteria exopolymers with iron using X-ray photoelectron spectroscopy and time-of-flight secondary ionisation mass spectrometry. J Microbiol Methods 36:3–10. doi:10.1016/S0167-7012(99)00005-6
11. Beekes M, Lasch P, Naumann D (2007) Analytical applications of Fourier transform-infrared (FT-IR) spectroscopy in microbiology and prion research. Vet Microbiol 123:305–319. doi:10.1016/j.vetmic.2007.04.010
12. Bellamy LJ (1975) The infra-red spectra of complex molecules. Chapman and Hall, London
13. Beney L, Mille Y, Gervais P (2004) Death of *Escherichia coli* during rapid and severe dehydration is related to lipid phase transition. Appl Microbiol Biotechnol 65:457–464. doi:10.1007/s00253-004-1574-x
14. Boonaert CJP, Dufrêne YF, Derclaye SR, Rouxhet PG (2001) Adhesion of Lactococcus lactis to model substrata: direct study of the interface. Colloids Surf B Biointerfaces 22:171–182. doi:10.1016/S0927-7765(01)00196-5

15. Bruinsma GM, van der Mei HC, Busscher HJ (2001) Bacterial adhesion to surface hydrophilic and hydrophobic contact lenses. Biomaterials 22:3217–3224. doi:10.1016/S0142-9612(01)00159-4

16. Burgula Y, Khali D, Kim S et al (2006) Detection of *Escherichia coli* O157:H7 and *Salmonella typhimurium* using filtration followed by Fourier-transform infrared spectroscopy. J Food Prot 69:1777–1784

17. Burgula Y, Khali D, Kim S et al (2007) Review of mid-infrared Fourier transform-infrared spectroscopy applications for bacterial detection. J Rapid Methods Autom Microbiol 15:146–175. doi:10.1111/j.1745-4581.2007.00078.x

18. Buszewski B (2015) Assignment of functional groups in Gram-positive bacteria. J Anal Bioanal Technol. doi:10.4172/2155-9872.1000232

19. Cadet F, de la Guardia M (2000) Quantitative analysis, infrared. In: Meyers RA (ed) Encyclopedia of analytical chemistry. Wiley, Chichester

20. Candeloro P, Tirinato L, Malara N et al (2011) Nanoparticle microinjection and Raman spectroscopy as tools for nanotoxicology studies. Analyst 136:4402–4408. doi:10.1039/C1AN15313G

21. Carlos C, Maretto DA, Poppi RJ et al (2011) Fourier transform infrared microspectroscopy as a bacterial source tracking tool to discriminate fecal *E. coli* strains. Microchem J 99:15–19. doi:10.1016/j.microc.2011.03.002

22. Cegelski L (2015) Bottom-up and top-down solid-state NMR approaches for bacterial biofilm matrix composition. J Magn Reson 253:91–97. doi:10.1016/j.jmr.2015.01.014

23. Chia BCS, Lam Y-H, Dyall-Smith M et al (2000) A31P NMR study of the interaction of amphibian antimicrobial peptides with the membranes of live bacteria. Lett Pept Sci 7:151–156. doi:10.1007/BF02443582

24. Choi O, Deng KK, Kim N-J et al (2008) The inhibitory effects of silver nanoparticles, silver ions, and silver chloride colloids on microbial growth. Water Res 42:3066–3074. doi:10.1016/j.watres.2008.02.021

25. Cieślik-Boczula K, Czarnik-Matusewicz B, Perevozkina M et al (2008) ATR-IR spectroscopic study of the structural changes in the hydrophobic region of ICPAN/DPPC bilayers. J Mol Struct 878:162–168. doi:10.1016/j.molstruc.2007.08.003

26. Coates J (2006) Interpretation of infrared spectra, a practical approach. In: Meyers RA (ed) Encyclopedia of analytical chemistry. Wiley, London

27. Colthup N (2012) Introduction to infrared and Raman spectroscopy. Elsevier, Amsterdam

28. Infrared Spectral Interpretation: A systematic approach. In: CRC Press. https://www.crcpress.com/Infrared-Spectral-Interpretation-A-Systematic-Approach/Smith/9780849324635. Accessed 13 December 2015b

29. Corte L, Rellini P, Roscini L et al (2010) Development of a novel, FTIR (Fourier transform infrared spectroscopy) based, yeast bioassay for toxicity testing and stress response study. Anal Chim Acta 659:258–265. doi:10.1016/j.aca.2009.11.035

30. Davis R, Mauer LJ (2010) Fourier transform infrared (FT-IR) spectroscopy: a rapid tool for detection and analysis of food-borne pathogenic bacteria. Curr Res Technol Educ Top Appl Microbiol Microb Biotechnol 2:1582–1594

31. Davis JH, Nichol CP, Weeks G, Bloom M (1979) Study of the cytoplasmic and outer membranes of *Escherichia coli* by deuterium magnetic resonance. Biochemistry (Mosc) 18:2103–2112. doi:10.1021/bi00577a041

32. Davis R, Irudayaraj J, Reuhs BL, Mauer LJ (2010) Detection of *E. coli* O157:H7 from ground beef using Fourier transform infrared (FT-IR) spectroscopy and chemometrics. J Food Sci 75:M340–M346. doi:10.1111/j.1750-3841.2010.01686.x

33. Dufrêne YF, Rouxhet PG (1996) X-ray photoelectron spectroscopy analysis of the surface composition of *Azospirillum brasilense* in relation to growth conditions. Colloids Surf B Biointerfaces 7:271–279. doi:10.1016/0927-7765(96)01295-7

34. Dufrêne YF, van der Wal A, Norde W, Rouxhet PG (1997) X-ray photoelectron spectroscopy analysis of whole cells and isolated cell walls of gram-positive bacteria: comparison with biochemical analysis. J Bacteriol 179:1023–1028

35. Eckhardt S, Brunetto PS, Gagnon J et al (2013) Nanobio silver: its interactions with peptides and bacteria, and its uses in medicine. Chem Rev 113:4708–4754. doi:10.1021/cr300288v

36. Fang J, Lyon DY, Wiesner MR et al (2007) Effect of a fullerene water suspension on bacterial phospholipids and membrane phase behavior. Environ Sci Technol 41:2636–2642. doi:10.1021/es062181w

37. Fang T-T, Li X, Wang Q-S et al (2012) Toxicity evaluation of CdTe quantum dots with different size on *Escherichia coli*. Toxicol In Vitro 26:1233–1239. doi:10.1016/j.tiv.2012.06.001

38. Feng QL, Wu J, Chen GQ et al (2000) A mechanistic study of the antibacterial effect of silver ions on *Escherichia coli* and *Staphylococcus aureus*. J Biomed Mater Res 52:662–668

39. Feo JC, Castro MA, Robles LC, Aller AJ (2004) Fourier-transform infrared spectroscopic study of the interactions of selenium species with living bacterial cells. Anal Bioanal Chem 378:1601–1607. doi:10.1007/s00216-004-2494-4

40. FT-IR Library: an essential reference for research. In: Sigma-Aldrich. http://www.sigmaaldrich.com/labware/learning-center/spectral-viewer/ft-ir-library.html. Accessed 24 December 2015a

41. Garidel P, Boese M (2007) Non-invasive Fourier transform infrared microspectroscopy and imaging techniques: basic principles and application. Mod Res Educ Top Microsc 1:132–143

42. Gericke A, Huehnerfuss H (1995) Investigation of Z- and E-unsaturated fatty acids, fatty acid esters, and fatty alcohols at the air/water interface by infrared spectroscopy. Langmuir 11:225–230. doi:10.1021/la00001a039

43. Gopal J, Manikandan M, Hasan N et al (2013) A comparative study on the mode of interaction of different nanoparticles during MALDI-MS of bacterial cells. J Mass Spectrom 48:119–127. doi:10.1002/jms.3135

44. Graves JL, Tajkarimi M, Cunningham Q et al (2015) Rapid evolution of silver nanoparticle resistance in *Escherichia coli*. Front Genet. doi:10.3389/fgene.2015.00042

45. Gurbanov R, Simsek Ozek N, Gozen AG, Severcan F (2015) Quick discrimination of heavy metal resistant bacterial populations using infrared spectroscopy coupled with chemometrics. Anal Chem 87:9653–9661. doi:10.1021/acs.analchem.5b01659

46. Hamadi F, Latrache H, Zahir H et al (2008) The relation between *Escherichia coli* surface functional groups' composition and their physicochemical properties. Braz J Microbiol Publ Braz Soc Microbiol 39:10–15. doi:10.1590/S1517-83822008000100003

47. Helm D, Labischinski H, Schallehn G, Naumann D (1991) Classification and identification of bacteria by Fourier-transform infrared spectroscopy. J Gen Microbiol 137:69–79. doi:10.1099/00221287-137-1-69

48. Holman H-YN, Miles R, Hao Z et al (2009) Real-time chemical imaging of bacterial activity in biofilms using open-channel microfluidics and synchrotron FTIR spectromicroscopy. Anal Chem 81:8564–8570. doi:10.1021/ac9015424

49. Hu C, Guo J, Qu J, Hu X (2007) Photocatalytic degradation of pathogenic bacteria with AgI/TiO$_2$ under visible light irradiation. Langmuir 23:4982–4987. doi:10.1021/la063626x

50. Hu X, Qiu Z, Wang Y et al (2009) Effect of ultra-strong static magnetic field on bacteria: application of Fourier-transform infrared spectroscopy combined with cluster analysis and

deconvolution. Bioelectromagnetics 30:500–507. doi:10.1002/bem.20506

51. Jiang W, Saxena A, Song B et al (2004) Elucidation of functional groups on gram-positive and gram-negative bacterial surfaces using infrared spectroscopy. Langmuir ACS J Surf Colloids 20:11433–11442. doi:10.1021/la049043

52. Jiang W, Yang K, Vachet RW, Xing B (2010) Interaction between oxide nanoparticles and biomolecules of the bacterial cell envelope as examined by infrared spectroscopy. Langmuir 26:18071–18077. doi:10.1021/la103738e

53. Jr TP (1995) All about albumin: biochemistry, genetics, and medical applications. Academic Press, Cambridge

54. Kačuráková M, Mathlouthi M (1996) FTIR and laser-Raman spectra of oligosaccharides in water: characterization of the glycosidic bond. Carbohydr Res 284:145–157. doi:10.1016/0008-6215(95)00412-2

55. Karatzas KAG, Bennik MHJ (2002) Characterization of a Listeria monocytogenes Scott a isolate with high tolerance towards high hydrostatic pressure. Appl Environ Microbiol 68:3183–3189. doi:10.1128/AEM.68.7.3183-3189.2002

56. Kenner BA, Riddle JW, Rockwood SW, Bordner RH (1958) Bacterial identification by infrared spectrophotometry II. J Bacteriol 75:16–20

57. Kinder R, Ziegler C, Wessels JM (1997) Gamma-irradiation and UV-C light-induced lipid peroxidation: a Fourier transform-infrared absorption spectroscopic study. Int J Radiat Biol 71:561–571. doi:10.1080/095530097143897

58. Kiwi J, Nadtochenko V (2005) Evidence for the mechanism of photocatalytic degradation of the bacterial wall membrane at the TiO2 interface by ATR–FTIR and laser kinetic spectroscopy. Langmuir 21:4631–4641. doi:10.1021/la046983l

59. Kollias N, Stamatas G (2002) Optical non-invasive approaches to diagnosis of skin diseases. J Investig Dermatol Symp Proc 7:64–75. doi:10.1046/j.1523-1747.2002.19635.x

60. Lamprecht C, Gierlinger N, Heister E et al (2012) Mapping the intracellular distribution of carbon nanotubes after targeted delivery to carcinoma cells using confocal Raman imaging as a label-free technique. J Phys Condens Matter 24:164206. doi:10.1088/0953-8984/24/16/164206

61. Larkin P (2011) Infrared and Raman spectroscopy: principles and spectral interpretation. Elsevier, London

62. Lasch P, Naumann D (2000) Infrared spectroscopy in microbiology. In:Meyers RA (ed) Encyclopedia of analytical chemistry. Wiley, London

63. Lay JO (2001) MALDI-TOF mass spectrometry of bacteria*. Mass Spectrom Rev 20:172–194. doi:10.1002/mas.10003

64. Leone L, Loring J, Sjöberg S et al (2006) Surface characterization of the Gram-positive bacteria Bacillus subtilis—an XPS study. Surf Interface Anal 38:202–205. doi:10.1002/sia.2184

65. Levine S, Stevenson HJR, Chambers LA, Kenner BA (1953) Infrared spectrophotometry of enteric bacteria. J Bacteriol 65:10–15

66. Lewis RN, McElhaney RN, Monck MA, Cullis PR (1994) Studies of highly asymmetric mixed-chain diacyl phosphatidylcholines that form mixed-interdigitated gel phases: Fourier transform infrared and 2H NMR spectroscopic studies of hydrocarbon chain conformation and orientational order in the liquid-crystalline state. Biophys J 67:197–207. doi:10.1016/S0006-3495(94)80470-9

67. Li J, Strong R, Trevisan J et al (2013) Dose-related alterations of carbon nanoparticles in mammalian cells detected using biospectroscopy: potential for real-world effects. Environ Sci Technol 47:10005–10011. doi:10.1021/es4017848

68. Li J, Ying G-G, Jones KC, Martin FL (2015) Real-world carbon nanoparticle exposures induce brain and gonadal alterations in zebrafish (Danio rerio) as determined by biospectroscopy techniques. Analyst 140:2687–2695. doi:10.1039/C4AN02227K

69. Liau SY, Read DC, Pugh WJ et al (1997) Interaction of silver nitrate with readily identifiable groups: relationship to the antibacterial action of silver ions. Lett Appl Microbiol 25:279–283

70. Lin M, Al-Holy M, Al-Qadiri H et al (2004) Discrimination of intact and injured Listeria monocytogenes by Fourier transform infrared spectroscopy and principal component analysis. J Agric Food Chem 52:5769–5772. doi:10.1021/jf049354q

71. Liu Z, Yang S, Bai Y et al (2011) The alteration of cell membrane of sulfate reducing bacteria in the presence of Mn(II) and Cd(II). Miner Eng 24:839–844. doi:10.1016/j.mineng.2011.03.005

72. Lopez Goerne MT (2011) Study of bacterial sensitivity to Ag–TiO2 nanoparticles. J Nanomed Nanotechnol. doi:10.4172/2157-7439.S5-003

73. Lorin-Latxague C, Melin A-M (2005) Radical induced damage of Micrococcus luteus bacteria monitored using FT-IR spectroscopy. J Spectrosc 19:17–26. doi:10.1155/2005/386404

74. Losasso C, Belluco S, Cibin V et al (2014) Antibacterial activity of silver nanoparticles: sensitivity of different Salmonella serovars. Front Microbiol. doi:10.3389/fmicb.2014.00227

75. Maquelin K, Kirschner C, Choo-Smith L-P et al (2002) Identification of medically relevant microorganisms by vibrational spectroscopy. J Microbiol Methods 51:255–271. doi:10.1016/S0167-7012(02)00127-6

76. Mariey L, Signolle JP, Amiel C, Travert J (2001) Discrimination, classification, identification of microorganisms using FTIR spectroscopy and chemometrics. Vib Spectrosc 26:151–159. doi:10.1016/S0924-2031(01)00113-8

77. Mauer LJ, Reuhs BL, Voeller JG (2008) Mid-infrared sensors for the rapid analysis of select microbial food borne pathogens. In: Voeller JG (ed) Wiley handbook of science and technology for homeland security. Wiley, London

78. Meier RJ (2005) Vibrational spectroscopy: a "vanishing" discipline? Chem Soc Rev 34:743. doi:10.1039/b503880d

79. Gué M, Dupont V, Dufour A, Sire O (2001) Bacterial swarming: a biochemical time-resolved FTIR–ATR study of proteus mirabilis swarm-cell differentiation. Biochemistry (Mosc) 40:11938–11945. doi:10.1021/bi010434m

80. Mille Y, Beney L, Gervais P (2002) Viability of Escherichia coli after combined osmotic and thermal treatment: a plasma membrane implication. Biochim Biophys Acta BBA Biomembr 1567:41–48. doi:10.1016/S0005-2736(02)00565-5

81. Moen B, Oust A, Langsrud Ø et al (2005) Explorative multifactor approach for investigating global survival mechanisms of Campylobacter jejuni under environmental conditions. Appl Environ Microbiol 71:2086–2094. doi:10.1128/AEM.71.4.2086-2094.2005

82. Moen B, Janbu AO, Langsrud S et al (2009) Global responses of Escherichia coli to adverse conditions determined by microarrays and FT-IR spectroscopy. Can J Microbiol 55:714–728. doi:10.1139/w09-016

83. Mossoba MM, Al-Khaldi SF, Jacobson A et al (2003) Application of a disposable transparent filtration membrane to the infrared spectroscopic discrimination among bacterial species. J Microbiol Methods 55:311–314. doi:10.1016/S0167-7012(03)00114-3

84. Mouwen DJM, Weijtens MJBM, Capita R et al (2005) Discrimination of enterobacterial repetitive intergenic consensus PCR types of Campylobacter coli and Campylobacter jejuni by Fourier transform infrared spectroscopy. Appl Environ Microbiol 71:4318–4324. doi:10.1128/AEM.71.8.4318-4324.2005

85. Mura S, Greppi G, Marongiu ML et al (2012) FTIR nanobiosensors for *Escherichia coli* detection. Beilstein J Nanotechnol 3:485–492. doi:10.3762/bjnano.3.55

86. Nadtochenko VA, Rincon AG, Stanca SE, Kiwi J (2005) Dynamics of *E. coli* membrane cell peroxidation during TiO2 photocatalysis studied by ATR–FTIR spectroscopy and AFM microscopy. J Photochem Photobiol Chem 169:131–137. doi:10.1016/j.jphotochem.2004.06.011

87. Naumann D (2006) Infrared spectroscopy in microbiology. In: Meyers RA (ed) Encyclopedia of analytical chemistry. Wiley, London

88. Naumann D, Schultz C, Sabisch A et al (1989) New insights into the phase behaviour of a complex anionic amphiphile: architecture and dynamics of bacterial deep rough lipopolysaccharide membranes as seen by FTIR, X-ray, and molecular modelling techniques. J Mol Struct 214:213–246. doi:10.1016/0022-2860(89)80015-8

89. Naumann D, Helm D, Labischinski H (1991) Microbiological characterizations by FT-IR spectroscopy. Nature 351:81–82. doi:10.1038/351081a0

90. Nelson BC, Petersen EJ, Marquis BJ et al (2013) NIST gold nanoparticle reference materials do not induce oxidative DNA damage. Nanotoxicology 7:21–29. doi:10.3109/17435390.2011.626537

91. Nydegger MW, Rock W, Cheatum CM (2011) 2D IR spectroscopy of the C–D stretching vibration of the deuterated formic acid dimer. Phys Chem Chem Phys PCCP 13:6098–6104. doi:10.1039/c0cp01087a

92. Ojeda JJ, Romero-Gonzalez ME, Bachmann RT et al (2008) Characterization of the cell surface and cell wall chemistry of drinking water bacteria by combining XPS, FTIR spectroscopy, modeling, and potentiometric titrations. Langmuir ACS J Surf Colloids 24:4032–4040. doi:10.1021/la702284b

93. Omoike A, Chorover J (2004) Spectroscopic study of extracellular polymeric substances from *Bacillus subtilis*: aqueous chemistry and adsorption effects. Biomacromolecules 5:1219–1230. doi:10.1021/bm034461z

94. Oren Z, Ramesh J, Avrahami D et al (2002) Structures and mode of membrane interaction of a short αhelical lytic peptide and its diastereomer determined by NMR, FTIR, and fluorescence spectroscopy. Eur J Biochem 269:3869–3880. doi:10.1046/j.1432-1033.2002.03080.x

95. Papadimitriou K, Boutou E, Zoumpopoulou G et al (2008) RNA arbitrarily primed PCR and fourier transform infrared spectroscopy reveal plasticity in the acid tolerance response of Streptococcus macedonicus. Appl Environ Microbiol 74:6068–6076. doi:10.1128/AEM.00315-08

96. Park H-J, Kim JY, Kim J et al (2009) Silver-ion-mediated reactive oxygen species generation affecting bactericidal activity. Water Res 43:1027–1032. doi:10.1016/j.watres.2008.12.002

97. Parker FS (1983) Applications of infrared, Raman, and resonance raman spectroscopy in biochemistry. Springer, Berlin

98. Perkins DL, Lovell CR, Bronk BV et al (2004) Effects of autoclaving on bacterial endospores studied by Fourier transform infrared microspectroscopy. Appl Spectrosc 58:749–753

99. Persson P, Nilsson N, Sjöberg S (1996) Structure and bonding of orthophosphate ions at the iron oxide-aqueous interface. J Colloid Interface Sci 177:263–275. doi:10.1006/jcis.1996.0030

100. Picquart M, Haro-Poniatowski E, Morhange JF et al (2000) Low frequency vibrations and structural characterization of a murine IgG2a monoclonal antibody studied by Raman and IR spectroscopies. Biopolymers 53:342–349. doi:10.1002/(SICI)1097-0282(20000405)53:4<342:AID-BIP6>3.0.CO;2-M

101. Pius J, Morrow MR, Booth V (2012) 2H solid-state nuclear magnetic resonance investigation of whole *Escherichia coli*

interacting with antimicrobial peptide MSI-78. Biochemistry (Mosc) 51:118–125. doi:10.1021/bi201569t

102. Podstawka-Proniewicz E, Piergies N, Skołuba D et al (2011) Vibrational characterization of L-leucine phosphonate analogues: FT-IR, FT-Raman, and SERS spectroscopy studies and DFT calculations. J Phys Chem A 115:11067–11078. doi:10.1021/jp207101m

103. Pradier CM, Rubio C, Poleunis C et al (2005) Surface characterization of three marine bacterial strains by Fourier transform IR, X-ray photoelectron spectroscopy, and time-of-flight secondary-ion mass spectrometry, correlation with adhesion on stainless steel surfaces. J Phys Chem B 109:9540–9549. doi:10.1021/jp044705p

104. Ramstedt M, Nakao R, Wai SN et al (2011) Monitoring surface chemical changes in the bacterial cell wall multivariate analysis of Cryo-X-ray photoelectron spectroscopy data. J Biol Chem 286:12389–12396. doi:10.1074/jbc.M110.209536

105. Reckel S, Löhr F, Dötsch V (2005) In-cell NMR spectroscopy. ChemBioChem 6:1601–1606. doi:10.1002/cbic.200500076

106. Reddy KM, Feris K, Bell J et al (2007) Selective toxicity of zinc oxide nanoparticles to prokaryotic and eukaryotic systems. Appl Phys Lett 90:213902-1–213902-3. doi:10.1063/1.2742324

107. Riddle JW, Kabler PW, Kenner BA et al (1956) Bacterial identification by infrared spectrophotometry. J Bacteriol 72:593–603

108. Riding MJ, Martin FL, Trevisan J et al (2012) Concentration-dependent effects of carbon nanoparticles in gram-negative bacteria determined by infrared spectroscopy with multivariate analysis. Environ Pollut 163:226–234. doi:10.1016/j.envpol.2011.12.027

109. Rizzello L, Pompa PP (2014) Nanosilver-based antibacterial drugs and devices: mechanisms, methodological drawbacks, and guidelines. Chem Soc Rev 43:1501–1518. doi:10.1039/C3CS60218D

110. Rodriguez-Saona LE, Khambaty FM, Fry FS et al (2004) Detection and identification of bacteria in a juice matrix with Fourier transform–near infrared spectroscopy and multivariate analysis. J Food Prot 67:2555–2559

111. Romaniuk JAH, Cegelski L (2015) Bacterial cell wall composition and the influence of antibiotics by cell-wall and whole-cell NMR. Philos Trans R Soc B 370:20150024. doi:10.1098/rstb.2015.0024

112. Rouxhet PG, Mozes N, Dengis PB et al (1994) Application of X-ray photoelectron spectroscopy to microorganisms. Colloids Surf B Biointerfaces 2:347–369. doi:10.1016/0927-7765(94)80049-9

113. Schanda P, Triboulet S, Laguri C et al (2014) Atomic model of a cell-wall cross-linking enzyme in complex with an intact bacterial peptidoglycan. J Am Chem Soc 136:17852–17860. doi:10.1021/ja5105987

114. Schifman LA, Kasaraneni VK, Sullivan RK et al (2015) New antimicrobially amended media for improved nonpoint source bacterial pollution treatment. Environ Sci Technol 49:14383–14391. doi:10.1021/acs.est.5b03782

115. Schleicher E, Heßling B, Illarionova V et al (2005) Light-induced reactions of *Escherichia coli* DNA photolyase monitored by Fourier transform infrared spectroscopy. FEBS J 272:1855–1866. doi:10.1111/j.1742-4658.2005.04617.x

116. Serber Z, Dötsch V (2001) In-cell NMR spectroscopy. Biochemistry (Mosc) 40:14317–14323. doi:10.1021/bi011751w

117. Shah N, Sattar A, Benanti M et al (2006) Magnetic resonance spectroscopy as an imaging tool for cancer: a review of the literature. J Am Osteopath Assoc 106:23–27

118. Shah NB, Dong J, Bischof JC (2011) Cellular uptake and nanoscale localization of gold nanoparticles in cancer using

label-free confocal raman microscopy. Mol Pharm 8:176–184. doi:10.1021/mp1002587

119. Sivakesava S, Irudayaraj J, Debroy C (2004) Differentiation of microorganisms by FTIR-AIR and NIR spectroscopy. Trans ASAE 47:951–957

120. Sprenger D, Anderson O (1991) Deconvolution of XPS spectra. Fresenius J Anal Chem 341:116–120. doi:10.1007/BF00322120

121. Tardy-Laporte C, Arnold AA, Genard B et al (2013) A 2H solid-state NMR study of the effect of antimicrobial agents on intact *Escherichia coli* without mutating. Biochim Biophys Acta BBA Biomembr 1828:614–622. doi:10.1016/j.bbamem.2012.09.011

122. Thi NAN, Naumann D (2006) Investigating the heterogeneity of cell growth in microbial colonies by FTIR microspectroscopy. Anal Bioanal Chem 387:1769–1777. doi:10.1007/s00216-006-0829-z

123. Tyler BJ (1997) XPS and SIMS studies of surfaces important in biofilm formation. Three case studies. Ann N Y Acad Sci 831:114–126

124. van der Mei HC, de Vries J, Busscher HJ (2000) X-ray photoelectron spectroscopy for the study of microbial cell surfaces. Surf Sci Rep 39:1–24. doi:10.1016/S0167-5729(00)00003-0

125. Whittaker P, Mossoba MM, Al-Khaldi S et al (2003) Identification of foodborne bacteria by infrared spectroscopy using cellular fatty acid methyl esters. J Microbiol Methods 55:709–716. doi:10.1016/j.mimet.2003.07.005

126. Wigginton NS, de Titta A, Piccapietra F et al (2010) Binding of silver nanoparticles to bacterial proteins depends on surface modifications and inhibits enzymatic activity. Environ Sci Technol 44:2163–2168. doi:10.1021/es903187s

127. Winder CL, Goodacre R (2004) Comparison of diffuse-reflectance absorbance and attenuated total reflectance FT-IR for the discrimination of bacteria. Analyst 129:1118–1122. doi:10.1039/b408169b

128. Yan L, Marzolin C, Terfort A, Whitesides GM (1997) Formation and reaction of interchain carboxylic anhydride groups on self-assembled monolayers on gold. Langmuir 13:6704–6712. doi:10.1021/la970762g

129. Yu C, Irudayaraj J (2005) Spectroscopic characterization of microorganisms by Fourier transform infrared microspectroscopy. Biopolymers 77:368–377. doi:10.1002/bip.20247

130. Yuan W, Jiang G, Che J et al (2008) Deposition of silver nanoparticles on multiwalled carbon nanotubes grafted with hyperbranched poly(amidoamine) and their antimicrobial effects. J Phys Chem C 112:18754–18759. doi:10.1021/jp807133j

131. Zeroual W, Choisy C, Doglia SM et al (1994) Monitoring of bacterial growth and structural analysis as probed by FT-IR spectroscopy. Biochim Biophys Acta BBA Mol Cell Res 1222:171–178. doi:10.1016/0167-4889(94)90166-X

132. Zhang H (2013) Application of silver nanoparticles in drinking water purification. University of Rhode Island, Rhode Island

133. Zhang H, Oyanedel-Craver V (2013) Comparison of the bacterial removal performance of silver nanoparticles and a polymer based quaternary amine functiaonalized silsesquioxane coated point-of-use ceramic water filters. J Hazard Mater 260:272–277. doi:10.1016/j.jhazmat.2013.05.025

134. 王雪飞 XW, Wang W, PL刘 鹏 et al (2011) Photocatalytic degradation of *E. coli* membrane cell in the presence of ZnO nanowires. J Wuhan Univ Technol Mater Sci Ed 26:222–225. doi:10.1007/s11595-011-0201-9